ELSEVIER

Journal of Nuclear Materials 301 (2002) 98–107

journal of nuclear materials

www.elsevier.com/locate/jnucmat

Tritium removal from codeposits on carbon tiles by a scanning laser

C.H. Skinner [a,*], C.A. Gentile [a], A. Carpe [a], G. Guttadora [a], S. Langish [a], K.M. Young [a], W.M. Shu [b], H. Nakamura [b]

[a] *Princeton Plasma Physics Laboratory, Princeton University, P.O. Box 451, James Forrestal Campus, Princeton, NJ 08543 USA*
[b] *Tritium Engineering Laboratory, JAERI, Ibaraki 319-1195, Japan*

Received 1 October 2001; accepted 10 December 2001

Abstract

A novel method for tritium release has been demonstrated on codeposited layers on graphite and carbon-fiber-composite tiles from the Tokamak Fusion Test Reactor. A scanning continuous wave Nd laser beam heated the codeposits to a temperature of 1200–2300 °C for 10–200 ms in an argon atmosphere. The temperature rise of the codeposit was significantly higher than that of the manufactured tile material (e.g. 1770 °C cf. 1080 °C). A major fraction of tritium was thermally desorbed with minimal change to the surface at a laser intensity of 80 W/mm^2, peak temperatures above 1230 °C and heating duration 10–20 ms. In two experiments, 46% and 84% of the total tritium was released during the laser scan. The application of this method for tritium removal from a tokamak reactor appears promising and has significant advantages over oxidative techniques.

1. Introduction

Tritium issues are central to the development of fusion power [1,2] and a significant milestone was reached when deuterium–tritium (DT) plasmas in the Tokamak Fusion Test Reactor (TFTR) and JET produced 10 and 16 MW of fusion power respectively [3,4]. A large fraction of tritium fuel was retained inside the vacuum vessel of both TFTR and JET, principally by codeposition with carbon eroded from plasma facing components [5–7]. In TFTR, several weeks were needed for tritium removal after only 10–15 min of cumulative DT plasmas. The amount of tritium retained in future DT machines with carbon plasma facing components will scale-up with the long pulse high duty-cycle operation. The time before the administrative safety limit for maximum tritium inventory is reached is uncertain but is of the order of a hundred pulses [1]. The subsequent availability of the machine for plasma operations will depend on efficient and fast tritium removal. Besides tritium inventory control, tritium removal from the vessel wall is required to control plasma fuelling by tritium implanted in the wall and to reduce the tritium outgassing during maintenance activities. Independent of safety limits, control of the in-vessel tritium inventory is also necessary to avoid exhausting the available tritium supply.

Significant progress in tritium removal technologies was made in support of the engineering design activities of the International Thermonuclear Experimental Reactor project (ITER) [2]. High temperature baking (>1000 K) under vacuum is sufficient to remove nearly all the trapped tritium [8], but is currently not technically possible for a large tokamak. Thermo-oxidative erosion at temperatures above 570 K, or oxygen plasma discharges have been found to be effective in laboratory experiments to remove tritium from tritium-containing films [9–12]. Major drawbacks of techniques using oxygen, especially at elevated temperature, include wall

* Corresponding author. Tel.: +1-609 243 2214; fax: +1-609 243 2265.
E-mail address: cskinner@pppl.gov (C.H. Skinner).

0022-3115/02/$ - see front matter
PII: S0022-3115(02)00713-4

conditioning time to subsequently remove oxygen and recover normal plasma operation, potential damage to in-vessel components, and the cost of processing large quantities of the DTO exhaust [13]. Some oxygen-free techniques have been proposed. Preliminary trials with CO_2 pellet blast cleaning removed the surface layer of a DIII–D tile, but also severely eroded the tile [14]. Cathodic arc cleaning has been used to remove codeposited carbon films from stainless steel and tungsten surfaces [15]. Potential methods to remove carbon flakes and dust are examined in Ref. [16]. No engineering-scale demonstration of tritium removal at the required rate has been performed to date on a tokamak.

Heating the tritiated codeposits by a scanning laser can release tritium without the deleterious effects of oxidation [17]. While bulk heating of a tokamak vacuum vessel to 1000 K under vacuum is impractical, the tritium is located on a surface film and only this film needs to be heated. A scanning laser is a convenient way to locally heat the surface. Multi-kW, robotically controlled lasers are a mature technology for industrial manufacturing. For application to a tokamak the laser would be external to the vessel and the beam coupled via fiber optics to a remotely controlled scanning device inside the vessel. Early work showed the release of hydrogen isotopes by heating with nanosecond pulses from electron beams and lasers [18–21]. More recently picosecond laser pulses were used for in situ measurements of hydrogen isotopes [22]. Excimer lasers have also been applied to tritium removal [23]. One issue with high power pulsed lasers is that ablation of the surface can exacerbate the tritium removal problem by distributing tritiated debris in inaccessible regions in a tokamak.

The purpose of this work is a proof-of-principal demonstration of tritium release from a codeposited film on TFTR tiles by heating with a scanning continuous laser beam in a laboratory experiment. The parametric dependencies of the tritium release on laser focal intensity, scanning speed, surface temperature and ambient gas, the release products and any morphological changes in the surface were studied to provide data for practical implementation in a tokamak.

2. Modeling

The temperature needed to release tritium depends on the transport of tritium in a codeposit at elevated temperatures, a process complicated by the porous, anisotropic structure of the codeposited layer. Tritium release in transient temperature excursions is sensitive to the slowest kinetics such as multistep low activation energy diffusion and is likely to be different to low temperature isochronal thermal desorption. The required laser intensity and exposure duration are governed by the thickness of the codeposited layer and the

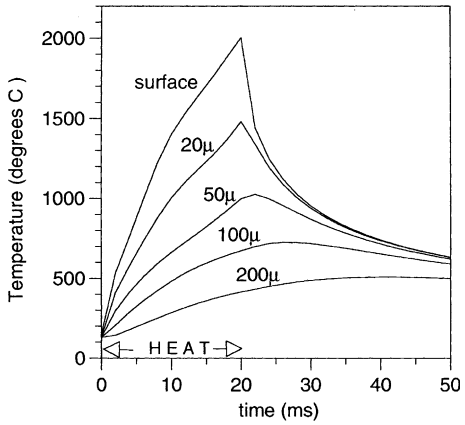

Fig. 1. Numerical calculation of temperature vs. time for pyrolytic perp. graphite under a 30 W/mm^2 heat flux for 20 ms. The curves represent the temperature at the depths indicated below the surface.

desired temperature excursion. Prior experiments [24] with a 30 ns pulsed ruby laser showed desorption of deuterium implanted in the top 100 nm of the surface at temperatures of order 1700 °C (depending on the type of graphite). Graphite and carbon-fiber-composite (CFC) materials are manufactured in a variety of forms and their thermal conductivity varies over a wide range depending on the microstructure and crystallite orientation. The thermal conductivity of amorphous carbon films has been measured at low (80–400 K) temperatures [25]. In the modeling, conductivity data for several forms of graphite and CFC was used, and 1700 °C was taken as the target temperature.

Fig. 1 shows results from numerical modeling of surface heating [17]. For the case of pyrolitic graphite with heat flow perpendicular to the layer planes, the surface temperature was predicted to reach 2000 °C after a 30 W/mm^2 heat pulse of duration 20 ms. At a depth 50 μm below the surface, the peak temperature is 926 °C. A laser power of order a few tens of W/mm^2 appears to be suitable for heating 50 μm codeposited layers.

3. Experimental setup

Multi-kW CO_2, neodymium (Nd) and diode lasers are available commercially. For the present proof-of-principle experiment we used a Nd laser system developed for laser marking purposes (Quantronix Corp. Model 118F/CW-325 with Q scan marking head). This is a multimode continuous wave laser with an output power up to 325 W at 1064 nm and with a specified beam divergence of 20 mrad. The output is steered by two galvanometer driven scanning mirrors that are pre-programmed via a PC computer and the beam is

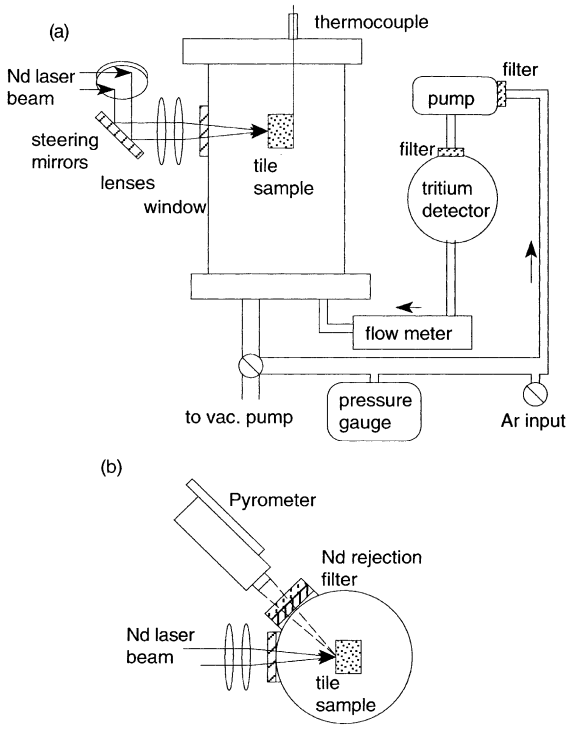

Fig. 2. Schematic of experimental setup shows: (a) the plan view and (b) the vertical cross-section with the pyrometer.

focussed inside a vacuum chamber containing a tile specimen (Fig. 2). The maximum laser intensity measured inside the tile chamber was 248 W. The original marking system had a working field of 150 mm × 150 mm field, with a maximum focal spot velocity of 4 m/s. For the present work, the focal intensity was increased by adding a second lens (combined focal length 125 mm). The scanning field was then 75 mm × 75 mm and maximum spot velocity 2 m/s. The focussed beam profile was too intense to measure with conventional beam profilers but a stationary laser spot 'drilled' a 1 mm diameter hole in graphite. For most of the experiments the cube surface was positioned 12 mm from the focal plane. At this point the focal spot was approximately 2 mm diameter, and the estimated focal intensity inside the chamber approximately 80 W/mm^2. A colinear helium neon laser beam indicated the location of the Nd laser spot.

Tiles that had been exposed to tritium plasmas during the TFTR DT campaign were retrieved from the vacuum vessel [26] and cut up into cubes of edge dimension approximately 2 cm. Both graphite (Union Carbide POCO AXF-5Q) and CFC tiles (Fiber Materials Inc. 4D coarse weave) were used. The tile cubes were placed in a 20 cm diameter stainless steel chamber that had two 7.6 cm diameter windows arranged at 45° for laser and pyrometer access. The laser access window was anti-reflection coated and the laser path was directed to a ceramic coated heat sink before and after each scan. The chamber was typically pumped and purged with argon 5 times, and then filled with 750 Torr of argon.

A pyrometer (Kleiber model 270B) viewed the tile surface at 45° to the Nd laser beam. It operated in the 1.58–1.8 μm spectral range and measured surface temperatures in the range 500–2300 °C with a specified accuracy of 1%. It was calibrated by the manufacturer with a 99.4% emissivity black body furnace with the vacuum window and Nd laser rejection filter (below) in place. The response time (to 99%) was 0.3 ms. Macro optics were used to define a 0.7 mm by 1 mm measuring spot which was positioned with a through-the-lens sighting system. To avoid any possibility of scattered 1.064 nm light from the laser affecting the measurement, a rejection filter with transmission less than 1% at 1.064 nm, 0–30° incidence and transmission greater than 80% at 1.4–1.8 μm was used. The spectral emissivity of graphite at 1.7 μm wavelength and 1578 °C was measured to be 0.91 [27]; however the emissivity depends on surface roughness and the emissivity of codeposits is unknown. We report the apparent brightness temperature as indicated by the pyrometer for a blackbody. The true temperature of a gray body with emissivity 0.9 and brightness temperature of 1500 °C would be 1530 °C; this is a small change compared to the experimental variations observed (Section 4.1). The signal from the pyrometer was recorded by a 12 bit PCI analog input board in the PC computer at a digitization rate typically 10 kHz. A thermocouple was placed at the back of the cube to record bulk temperature changes.

Before and after each experiment the codeposited surface was imaged at normal incidence and at 45° with a digital microscope (National Optical & Scientific Instruments Model DC3-420T). This microscope was also used to make video recordings of the incandescence from the laser spot on the cube.

Tritium release was measured in several ways. The principal instrument was an ion chamber (Fempto-Tech model 252400) [28] that recorded the tritium concentration in a closed loop circulation system. The dynamic range for this instrument is 1–20,000 Ci/m^3. The response is known to be different for different carrier gases because of differences in collision rates. The ion chamber was calibrated by releasing a small quantity of tritium at low laser power and flowing the gas through both the ion chamber and a Scintrex 209 tritium monitor in series in a closed loop. The Scintrex monitor is calibrated with standard gas containing 250 μCi/m^3 of tritium. A second calibration was performed by inserting an envelope containing a molecular sieve into the loop. This absorbs HTO, which is subsequently measured by liquid scintillation counting. The tritium absorbed by the molecular sieve was then compared to the decrease in the ion

chamber reading. These two independent methods gave calibration factors within 10%, that were also consistent with earlier work on ion chamber calibration [29]. The calibration showed that for an argon atmosphere the true tritium concentration was the ion chamber reading times a factor of 0.54. For air, the factor was $\times 0.69$.

A differential atmospheric tritium sampler (DATS) [30] was used to measure the released HTO and HT fractions separately. The DATS absorbs HTO on a molecular sieve, and then oxidizes the HT with a palladium catalyst and absorbs this fraction on a separate molecular sieve. Before and after laser exposure, tritium activity on the surface of the cube was measured with an open wall ion chamber [31]. Any tritiated debris on the interior of the tile chamber was collected with cotton swabs and the tritium measured with a liquid scintillation counter.

4. Tritium release experiments

A total of 12 cubes have been scanned by the Nd laser to date. These were cut from CFC tiles KC15, KC17 and graphite tile KC22 from TFTR. Designator 'KC17 3D' indicates a cube cut from a TFTR tile from bay K, column C, row 17 [6] and the cube is from the 3rd row up 4th column to the right. An open wall ion chamber [31] was used to map the tritium distribution on tile KC17 before sectioning to cubes. The detector area was 6 mm diameter and the detector is sensitive to tritium in the top micron of the surface. The areal tritium density ranged between 0.6 and 1.9 Ci/m^2 with an average of 1.06 Ci/m^2.

A typical experiment proceeded as follows. After the cube was loaded in the chamber, it was connected to the pumping system and pump/purged 5 times with argon to change the atmosphere to argon. Cross hairs in the telescopic sight on the pyrometer were aligned to the colinear helium neon laser spot on a surface typically positioned 12 mm in front of the Nd laser focal plane. Burn paper was used to detect and compensate for any misalignment between the helium neon and Nd lasers. The laser chamber was then brought into position and as evidenced by the helium laser spot on the cube surface reappearing in the pyrometer cross hairs, as in Fig. 2(b). The helium neon laser was then scanned with a rectangular test pattern that was adjusted to define the border of the cube in terms of the programming parameters. Raster patterns on different areas of the cube surface were then programmed and tested by visual observation with the helium neon laser. These scanned either vertically or horizontally over specific areas of the cube surface with a line spacing typically 0.5 mm (Fig. 3). Since this spacing is less than the focal spot size a given position on the cube experienced first the fringe, then the center and then again the fringe of the laser spot in about six passes (Fig. 4). To allow time to turn the Nd

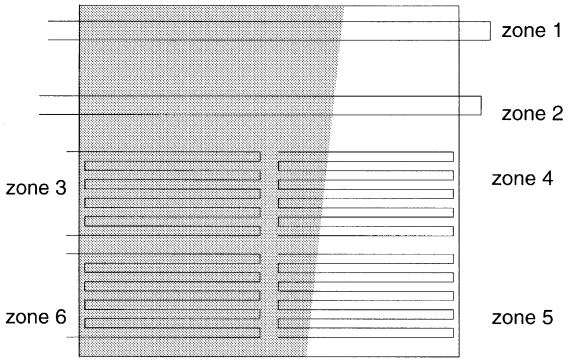

Fig. 3. Schematic of Nd laser raster pattern used on KC17 cube 2B (Fig. 6). Zone one and two are line patterns were used for video recording of the laser interaction (Fig. 10). The lower four patterns measured the response of the different textured surfaces to the laser at powers of 91 and 242 W.

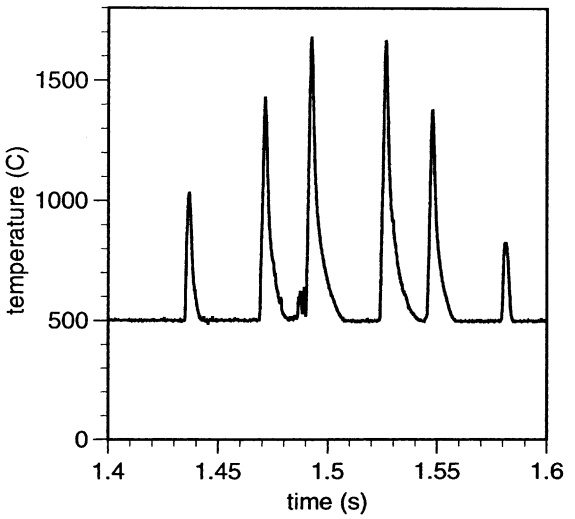

Fig. 4. Temperature history of the location viewed by the pyrometer during a raster scan for laser 80 W/mm^2, scan speed 1000 mm/s on KC17 cube 1C.

laser on and off, the program aimed the laser at the heat sink at the back of the laser chamber for 10 s before and after the raster scan. The PC digitizer was triggered just before the scan and the pyrometer data recorded. The scanning laser beam, viewed through laser safety glasses, produced a dazzlingly bright spot on the surface. The released tritium was circulated through the ion chamber which increased to a steady value over a few minutes.

4.1. Variation of temperature rise with surface material

The conductivity of the codeposits is not known but is likely to be low because of its open porous structure [32]. This is advantageous for laser heating, as the

temperature rise is higher and more localized to the codeposit. There are microscopic variations in temperature within the laser focal spot (see Section 4.3) so that the reported temperature represents an average within the 0.7 mm viewing spot of the pyrometer. Fig. 5 shows a comparison between the thermal response of a codeposit and the underlying graphite. In both experiments the laser intensity was 80 W/mm^2, scan speed 1000 mm/s, and atmosphere argon. The response of the codeposited side was measured first, and then the cube was rotated to bring the side cut by the saw to face the Nd laser. The peak temperature of the codeposited side was 1770 °C, much higher than the 1080 °C measured for the graphite surface revealed by the sawcut.

Another cube, cut from a CFC tile showed an interesting feature (Fig. 6) where part of the surface had a darker appearance, without much codeposit. The temperature response was measured by aligning the pyrometer on the left and then the right of the front surface of the cube for laser scan conditions 80 W/mm^2, scan speed 50 mm/s, and atmosphere of argon. The peak temperature on the left was 1841 °C compared to 1181 °C on the right confirming that the temperature rise was very dependent on the surface morphology.

The emissivity may also change with the surface texture. To check the influence of the emissivity on the temperature measurement the adjacent cube (KC17-2A) was heated to 600 °C for several minutes by a defocussed continuous Nd laser spot. Spatially scanning the pyrometer from left to right over the different surface

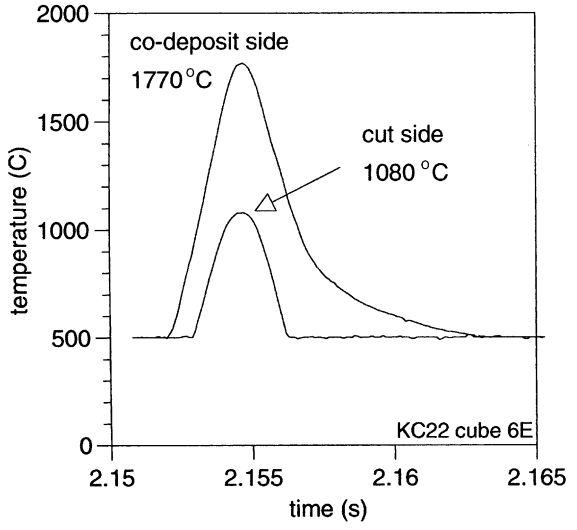

Fig. 5. Comparison of the large difference between the thermal response of a codeposited layer and the graphite substrate to the Nd laser. The experimental conditions were the same in both cases, except that either the codeposited side or cut side faced the Nd laser. Note the pyrometer does not read below 500 °C.

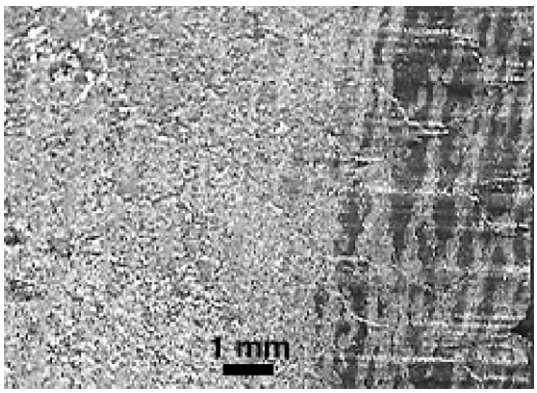

Fig. 6. Light microscope image of different surface textures on codeposit on KC17 cube 2B.

textures showed a change of only 19° so changes in emissivity cannot account for the large change above. The CFC material, being a 4D weave, is expected to be approximately thermally isotropic. The highest temperature rise (slightly over 2300 °C, the limit of the pyrometer) was seen for cube KC17-2G which had a thick codeposit. In contrast, cube KC15-21C had a codeposit much smoother in appearance, and a scan at the same laser power and scan speed (80 W/mm^2, 1000 mm/s) resulted in a peak temperature of only 1381 °C and released much less tritium (Section 4.4).

In one case (KC17-4E) the Nd laser scanned the surface that originally faced the gap between tiles on the TFTR bumper limiter. A band approximately 1 cm wide, adjacent to the plasma facing surface showed the appearance of codeposition [33]. This experiment was performed before the full diagnostics were available, but visually there was a much more intense interaction of the Nd laser in the codeposition region. In general, codeposits on graphite and CFC tiles behaved similarly. The temperature rise depends strongly on the morphology of the surface layer with codeposited surfaces reaching much higher temperatures than the manufactured material.

4.2. Temperature rise vs. scan speed

The depth of heat penetration depends on the duration of the exposure which is controlled by varying the scan speed. For a fixed laser power of 80 W/mm^2 and argon atmosphere, the scan speed was varied from 50 to 2000 mm/s in a sequence of raster scans on two cubes (Fig. 7). The raster was moved to a fresh area for each scan. For an idealised homogeneous material, the temperature rise would scale with the square root of the heat pulse duration. The peak temperature deviates markedly from this relation below scan speeds of 1000 mm/s as additional heat absorption mechanisms become active.

To compare the evolution of the surface temperature at different scan speeds, the time evolution recorded by

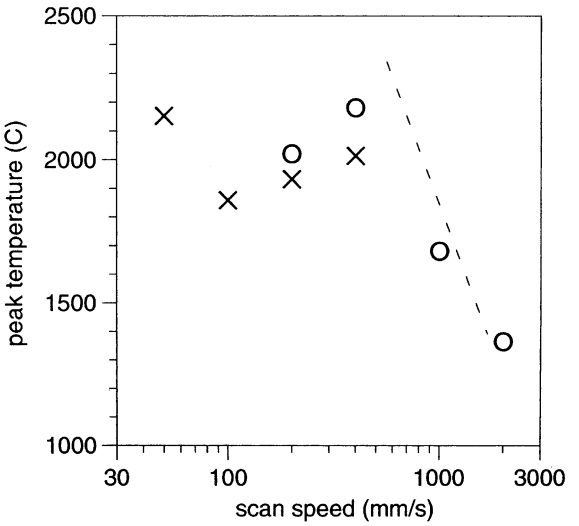

Fig. 7. Peak temperature vs. scan speed for two cubes: circles are KC17 cube 1C and crosses KC17 cube 4C. The dashed line represents an idealized inverse square root dependence of peak temperature on scan speed.

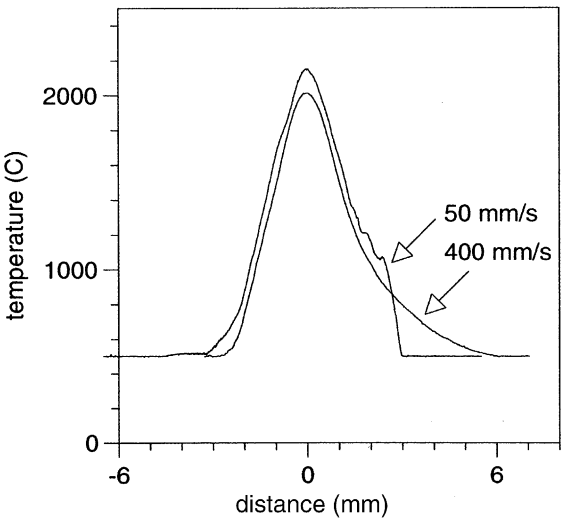

Fig. 8. Temperature recorded by pyrometer on KC17 cube 4C at scan speeds of 50 and 400 mm/s. The horizontal axis represents the distance between the pyrometer viewing spot and the scanning laser spot. The peak temperature is similar, but there is a sharp temperature decrease at 50 mm/s, possibly caused by ejection of material exposing the cooler substrate.

the pyrometer was converted to a spatial variation by multiplying the elapsed time by the scan speed. Fig. 8 shows a comparison of temperature evolution at scan speeds of 50 and 400 mm/s. The steep temperature drop at the lower speed is likely caused by ejection of material exposing the cooler substrate. It appears that at slow speeds laser energy is going to material ablation. The spatial transition between the more insulating codeposit and the more conducting substrate will also affect the dependence of temperature on heat pulse duration. The temperature of the back side of the cube was measured by a thermocouple and typically rose by 5–10 °C.

4.3. Microscope images of the surface before, during and after the laser scan

Microscope images were taken of each cube before and after the laser scan. The cubes were viewed normal to the surface and at 45°. Fig. 9 shows a cube before and after a fast laser scan 1000 mm/s at full laser power, 80 W/mm^2 in an argon atmosphere. There is slight color change as a result of the laser scan but the codeposit appears undisturbed even though the surface temperature reached 1770 °C and 18 mCi of tritium was released (Section 4.5). The duration of the heat pulse at this scan speed is approximately 10 ms (Fig. 5). These conditions are a good match to the modeling predictions for the heat flux needed to heat a 50 μm thick layer to above 1000 °C (Section 2).

The digital microscope could be configured to record videos at 30 frames/s. Fig. 10 shows four still images from a video taken through a $\times 100\,000$ neutral density filter of the intense incandescence from the interaction of the Nd laser with the surface of cube KC17-2B. In this case the scan speed was 50 mm/s. There is some elongation of the image in the horizontal direction due to the finite shutter open time. It is clear that the interaction is not uniform and 100–400 μm hot spots are apparent. Microscopic variations of the thermal conduction from surface grains to the underlying material lead to large spatial variations in temperature and the temperature recorded by the pyrometer then is an average over these hot spots within the 0.7 mm viewing area of the pyrometer. The incandescence is much brighter in Fig. 10 (a) and (b) taken from the light gray area (seen on the left side of Fig. 6), consistent with the pyrometer measurements (Section 4.1).

The thermal response of plasma facing materials is typically calculated with coefficients for bulk materials; for example to check if the maximum temperature is below the threshold for radiation induced sublimation. These images illustrate very clearly that the thermal response depends on the microstructure of the codeposit and reliable predictions for deposition areas need to be based on experiments with tokamak generated codeposits.

4.4. Tritium release in air or argon atmospheres

The atmosphere in the vacuum chamber was circulated through an ion chamber that measured the tritium

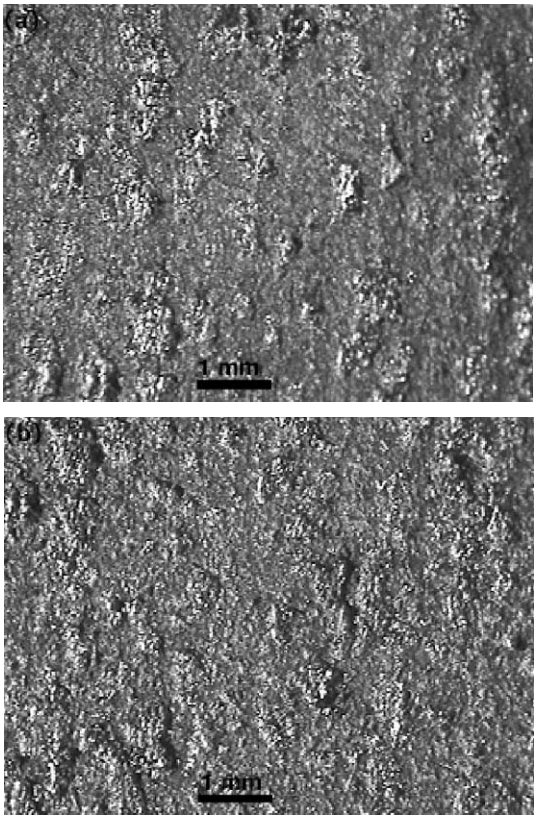

Fig. 9. Microscope images taken normal to the surface of KC17 cube 6E surface before (a) and after (b) a Nd laser scan (80 W/mm^2, 1000 mm/s). At this high scan speed there is very little difference in the appearance even though the surface was heated to 1770 °C (Fig. 5) by the laser and 18 mCi of tritium released.

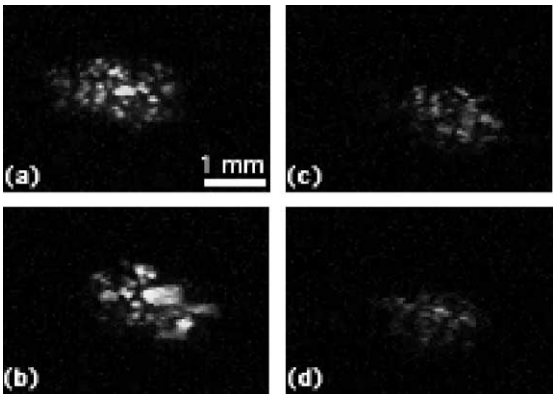

Fig. 10. Still images from a video taken of the Nd laser interacting with the surface of KC17 cube 2B. The laser power was 80 W/mm^2, atmosphere argon, and the scan was in the horizontal direction at a speed of 50 mm/s. Frames (a) and (b) are from the left, light gray area as seen in Fig. 6, frames (c) and (d) are from the blacker area on the right. The light emission was attenuated by $\times$l00 000 with a neutral density filter. Micro-'hot spots' are evident. The scale bar in (a) applies to all frames.

Table 1
Comparison of tritium release in argon and air (KC17 cube IE)

Atmosphere	Ion chamber (mCi)	DAT HTO (mCi)	DAT HT (mCi)
Air	8.3	4.8	0.7
Argon	6.9	1.0	Not measured

concentration. The total tritium release was then calculated by multiplying the concentration by the total volume of the system. The role of the ambient gas on the products of the laser interaction was measured in sequential experiments in air and argon. The left hand side of the codeposited surface on a cube was scanned by the Nd laser (80 W/mm^2, 50 mm/s) in an atmosphere of room air and the tritium release recorded. After the ion chamber reading was steady, a DATS [30] was inserted into the circulation loop and was used to measure the HTO and HT. The atmosphere in the chamber was then purged with argon 5 times and the right hand side of the cube surface scanned by the Nd laser with identical laser parameters. Sampling with a residual gas analyzer showed 99% of the gas to be argon. The tritium release was measured as before, except that only the HTO could be measured by the DATS, as no external oxygen was available to oxidize the HT. The results are shown in Table 1. With an air atmosphere, the major fraction of tritium is released in the oxide form. With an argon atmosphere this fraction is much less, but not zero. While oxygen and water vapor are excluded from the chamber, oxides have been detected in the tile surface by X-ray photoelectron spectroscopy with an oxygen atomic concentration (excluding H-isotopes) of 20–50% [34]. This presumably originates from water absorption by the tile from air humidity in the 4-year period after the termination of plasma operations on TFTR. In an operating tokamak, wall conditioning techniques are used to remove oxygen from the plasma facing surfaces and the HTO fraction in the release is expected to be very small. It can be seen that the total tritium (HTO + HT) measured by the DATS is less that measured by the ion chamber. The discrepancy could be caused by wall absorption or the presence of tritiated hydrocarbons that were not oxidized by the catalyst.

Any debris from the laser interaction that coated the inside walls of the test chamber was collected by a Q-tip swab and the tritium content measured in a liquid scintillation counter. Extrapolating the sampled area to the whole inside surface of the vacuum chamber typically gave an total of 1–3 μCi. This is very small compared to the tens of mCi released.

4.5. Tritium release vs. peak temperature

Fig. 11 shows a plot of the released tritium as a function of the peak temperature on the tile surface. The laser power was 80 W/mm^2 and atmosphere argon. A fresh surface was used for each scan which covered 1/4 of the cube area. Much of the scatter in the data is due to the non-uniformity of tritium across the tile. An early experiment, done before the in-line ion chamber was in place, used a lower intensity focal spot of approximately 10–20 W/mm^2 on KC17 cube 4E. The peak temperature was 1230 °C, maximum duration above 500 °C was 95 ms and the surface tritium activity decreased only from 0.76 to 0.51 Ci/m^2. The temperature threshold is not precisely defined by the data, but it appears temperatures above 1230 °C are needed to release large fractions of tritium.

4.6. Tritium release vs. heat pulse duration

The heat penetration depth was controlled by varying the local heating time through the scan speed. Since the pyrometer viewed a 0.7 mm spot, the spacing between lines in the raster was set to 0.5 mm to ensure the peak temperature was recorded. The overall laser spot diameter was approximately 2 mm and this meant that a given point would first experience the fringe of the laser spot, then successive passes would bring the spot across the pyrometer view area generating several temperature excursions of increasing, then decreasing peak temperature (Fig. 4). Repeating a raster on the same area of KC17 cube 4C released 1.7 mCi on the first scan and then 0.14 mCi. For KC22 cube 6E a larger area raster had a line spacing of 1 mm and this was then repeated with the pattern shifted by 0.5 mm. The tritium released was 12.1 mCi in the first raster and 2.2 mCi in the second. With this spacing the pyrometer recorded two excursions above 1000 °C. It appears that most of the tritium is released in one or two heat pulses. Fig. 12 plots the maximum duration the pyrometer temperature was above 500 °C in a single pass. It can be seen that the tritium release is not a strong function of the duration. A heating pulse of order 10 ms and temperature excursion to 1500 °C seems optimal for removing tritium with minimal change to the surface morphology. The 10 ms duration is consistent with heat penetration through a 50 μm thick codeposit (Section 2). Measurements of the thickness of the codeposited layer on this tile are not yet available; however previous measurements of deuterium codeposits from TFTR were of a 50 μm scale [32].

4.7. Residual tritium

Baking in air at temperatures above 350 °C is known to remove almost all the tritium from a codeposited layer [8] and this technique was used on two cubes to measure tritium remaining after a laser scan. The plasma facing surface of KC22 cube 6E was scanned by the laser at 80 W/mm^2, scan speed 1000 mm/s. The maximum temperature was 1770 °C and 18 mCi of tritium was released. Measurements of surface tritium with an open wall ion chamber showed the areal concentration decreasing from 0.99 to 0.29 Ci/m^2. The cube was rotated 90° and heated to 450 °C for 40 min in air with a stationary defocussed

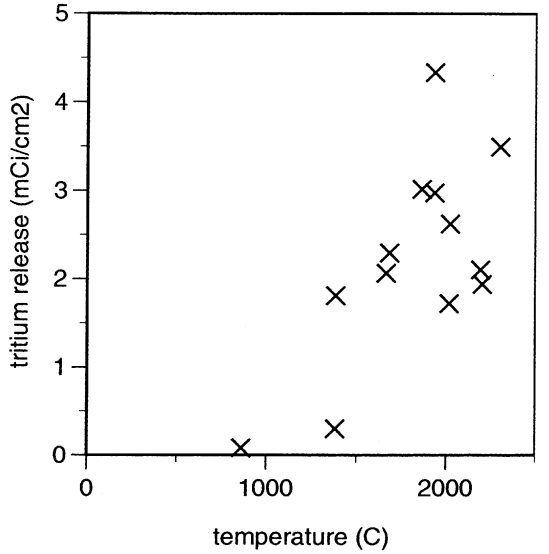

Fig. 11. Tritium released vs. peak temperature on tile surface. The plot shows data from cubes: KC17-3C, KC17-4C, KC17-1C, KC17-2G and KC15-21C.

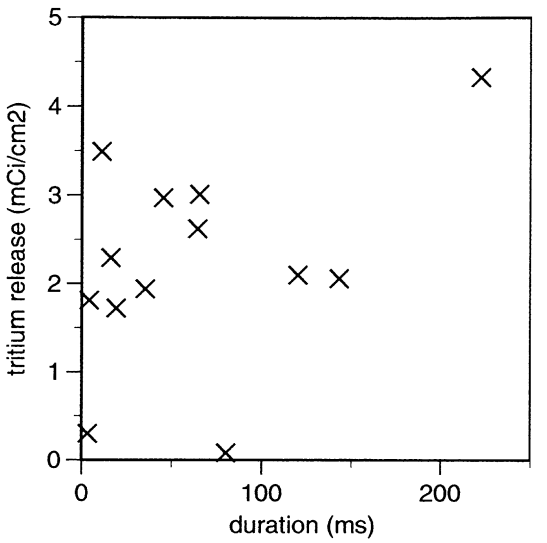

Fig. 12. Tritium release vs. maximum duration of temperature excursion above 500 °C. The plot shows data from cubes: KC17-3C, KC17-4C, KC17-1C, KC17-2G and KC15-21C.

100 W Nd laser beam to release the remaining tritium by oxidation. The temperature was measured by a thermocouple on the back side of the cube. This laser 'bake' released 21 mCi of tritium and the surface tritium decreased from 0.29 Ci/m^2 to zero. The fraction of the total tritium that was released by the laser scan was then 46%.

In the experiments described above the cube surface was positioned 12 mm from the focal plane of the laser. The next cube (KC22 cube 6C) was positioned at the focal plane and focussed laser intensity estimated at 310 W/mm^2. The surface temperature peaked at 2031 °C and the raster created visible tracks on the surface indicating some loss of surface material. The scan was repeated three times releasing 22.6, 3.3 and 1.9 mCi, i.e. a total of 28 mCi. The subsequent bake released only 5.3 mCi, so that the fraction of the total tritium released by the laser scan was encouragingly high at 84%.

The Nd laser is multimode and the intensity profile at the focus likely to be irregular. In the future we plan to use a fiber optic to transmit the laser beam to the scan head and this should help smooth and control the focal intensity and release a high fraction of the tritium with minimal change to the morphology of the codeposited surface.

5. Applications

The measurements reported above indicate a strong potential for laser scanning to remove tritium from codeposited layers in a DT next-step device. In a scaled-up system we envisage a multi-kW laser beam delivered via fiber optics to a scanning head on a robotic arm or a mobile robot inside the vessel. A line focus would be convenient for covering large areas of tile. Energetically, 30 MJ are needed to heat the top 100 μm of a 50 m^2 codeposited area from 400 to 2000 °C and this corresponds to the output of a 3 kW laser for 3 h. Areas in the gaps in between tiles would need specialized optics to deliver the beam. The temperature excursion would also release volatile impurities from the tiles and improved wall conditioning may prove a significant collateral benefit to subsequent plasma operations. Clearly much work remains to be done to develop this technique at an engineering scale; however the initial results show clearly that tritium can be released without the deleterious effects of oxidation.

Plasma facing components in a tokamak experience high heat fluxes in off normal events such as ELMs and disruptions. E-beams, plasma devices and lasers are used to simulate these effects in the laboratory [2]. The different thermal response of a codeposit compared to the manufactured graphite, clearly evident in this work, underlines the fact that the morphology and composition of plasma facing surfaces are determined by the discharges in the tokamak and have properties different to the manufactured components. It is important to test the effects of disruptions on realistic codeposits. A laser intensity of 80 W/mm^2 for 200 ms duration resulted in major surface damage (in contrast to short exposure times that cause minimal change to the surface (Fig. 9)). In comparison a disruption in ITER is expected to generate a heat flux two orders of magnitude higher (10–100 MJ/m^2 in 1–10 ms) although >90% of this will be dispersed by vapor shielding [2]. Previous disruption simulation experiments [35,36] used pulsed lasers of 0.1–0.3 ms duration. A scanning focussed laser beam offers a new way to study the interaction of very high heat fluxes with tokamak generated codeposits at relevant durations.

In summary, a major fraction of the tritium trapped in a codeposited layer during the DT campaign on TFTR was released by heating with a scanning laser beam. This technique offers the potential for tritium removal in a next-step DT device without the use of oxidation and the associated deconditioning of the plasma facing surfaces and the expense of processing large quantities of tritium oxide.

Acknowledgements

We wish to acknowledge informative discussions with D. Cahill, R. Causey, J. Davis, G. Federici, A.A. Haasz, A. von Keudell, R-D. Penzhorn, R. Reichle, and the dedicated work of the tritium group and collaborators at PPPL. We thank J. Dong, A. Planetta and the PPPL health physics group for supporting these measurements. Financial support was provided by the Annex IV to the JAERI/DOE Implementing Arrangement on Cooperation in Fusion Research and Development, and US DOE Contract Nos. DE-AC02-76CH0307.

References

[1] G. Federici et al., J. Nucl. Mater. 290–293 (2001) 260.
[2] G. Federici, C.H. Skinner et al., Plasma-material Interactions in Current Tokamaks and their Implications for Next-step Fusion Reactors, joint report by the Princeton Plasma Physics Laboratory and the Max-Planck-Institut für Plasmaphysik, PPPL-3531/IPP-9/128 January 2001, Nucl. Fusion 41 (2001) 1967.
[3] A. Gibson et al., Phys. Plasmas 5 (1998) 1839.
[4] R.J. Hawryluk, Rev. Mod. Phys. 70 (1988) 537.
[5] C.H. Skinner et al., J. Vac. Sci. Technol. A 14 (1996) 3267.
[6] C.H. Skinner et al., J. Nucl. Mater. 290–293 (2001) 486.
[7] P. Andrew et al., Fusion Eng. Des. 47 (1999) 233.
[8] R.A. Causey, W.R. Wampler, D. Walsh, J. Nucl. Mater. 176&177 (1990) 987.
[9] W. Wang, W. Jacob, J. Roth, J. Nucl. Mater. 245 (1997) 66.
[10] J.W. Davis, A.A. Haasz, J. Nucl. Mater. 266–269 (1999) 478.

[11] K. Maruyama, W. Jacob, J. Roth, J. Nucl. Mater. 264 (1999) 56.
[12] S. Alberici et al., J. Nucl. Mater. 266–269 (1999) 754.
[13] C.H. Skinner et al., Nucl. Fusion 39 (1999) 271.
[14] R.E. Nygren, personal communication.
[15] K.J. Hollis, R.G. Castro, C.J. Maggiore, A. Ayala, Nucl. Mater. 283 B (2000) 1085.
[16] G.F. Counsell, C.H. Wu, Phys. Scripta T91 (2001) 70.
[17] C.H. Skinner et al., Proceedings of the 17th IEEE/NPSS Symposium Fusion Engineering, San Diego, CA, 6–10 October 1997, p. 321.
[18] B.L. Doyle, F.L. Vook, J. Nucl. Mater. 85&86 (1979) 1019.
[19] S.T. Picraux, W.R. Wampler, J. Nucl. Mater. 93&94 (1980) 853.
[20] B. Terreault, J. Appl. Phys. 62 (1986) 152.
[21] H.Y. Guo, B. Terreault, Rev. Sci. Instr. 64 (1993) 700.
[22] D.D.R. Summers et al., J. Nucl. Mater. 290–293 (2001) 496.
[23] W.M. Shu et al., Tritium decontamination of TFTR D_T plasma facing components using ultra violet laser, in: Proceedings of 6th International Conference on Tritium Science and Technology, November 11–16, 2001, Tsukuba, Japan, Fus. Eng. Des. 41 (Mar. 2002) in press.
[24] D. Keroack, B. Terreault, J. Nucl. Mater. 231 (1996) 47.
[25] A.J. Bullen et al., J. Appl. Phys. 88 (2000) 6317.
[26] C.H. Skinner et al., J. Nucl. Mater. 290–293 (2001) 486.
[27] G. Neuer, Int. J. Thermophys. 16 (1995) 257.
[28] N.P. Kherani, W.T. Shmayda, Fusion Tech. 21 (1992) 340.
[29] A. Nagy et al., Proceedings of the 17th IEEE/NPSS Symposium Fusion Engineering, San Diego, CA, 6–10 October 1997, p. 317.
[30] O.A. Griesbach, J.R. Stencel, Proceedings of the 22nd Midyear Symposium of the Health Physics Society, San Antonio, TX, December 1988, p. 374.
[31] N.P. Kherani, W.T. Shmayda, Fusion Tech. 28 (1995) 893.
[32] B.E. Mills et al., J. Nucl. Mater. 162–164 (1989) 343.
[33] W.R. Wampler et al., J. Vac. Sci. Technol. A 6 (1988) 2111.
[34] M.T. Paffett, S. Willms, C Gentile, C.H. Skinner, Surface characterization of TFTF first wall graphite tiles used during DT operations, in: Proceedings of 6th International Conference on Tritium Science and Technology, November 11–16, 2001, Tsukuba, Japan, Fus. Eng. Des. 41 (Mar. 2002) in press.
[35] J.P. Quian et al., J. Nucl. Mater. 196–198 (1992) 653.
[36] J.G. van der Laan et al., J. Nucl. Mater. 196–198 (1992) 612.